scientific reports

OPEN

Gender differences in L1 vertebral strength in adults 50+ using automated CT-based finite element analysis

Hsiang-Ho Chen[1,2,4], Chieh-Wei Wu[1,4], Yen Cheng[3], Mao-Chieh Su[1], Yu-Jhen Chen[1] & Po-Liang Lai[2✉]

Osteoporosis is usually diagnosed using a Bone Mineral Density test using dual-energy X-ray Absorptiometry. However, it is limited by low testing rates and the inability to directly measure bone strength. Finite Element Analysis allows for a more detailed assessment of bone strength. However, its modeling complexity and high computational time requirements pose challenges. This study aims to develop customized MATLAB programs to automate the creation of heterogeneous bone models, streamlining preprocessing to reduce time, computational costs, and minimize variability from manual processes. The focus is on establishing a prediction model for the structural strength of the L1 vertebral body using patient-specific CT data, thereby aiding in the prediction of vertebral fracture risk. The CT images are stacked into a 3D array, and the pixel values are converted by Hounsfield units based on CT image. The bone segment and elasticity values are established based on the Hounsfield units. After modeling, strain and stress analysis were performed through the solver LS-DYNA. The compression force was distributed vertically on the upper endplate of the vertebral body. All nodes in the subvertebral plane were fully constrained. For comparison, vertebral models were automatically established and analyzed from recruited subjects. This study collected spine CT imaging datasets from 52 subjects, comprising 28 males and 24 females aged between 50 and 95 years. Preprocessing and mechanical analysis for each subject took an average of approximately 579.6 seconds. Analysis of the results indicated that women over 50 years of age exhibited higher strain and stress values in their vertebral models compared to men under the same applied force, highlighting gender-specific differences in biomechanical characteristics. This study effectively employed a practical approach to identify and select specific spinal segments from CT images, facilitating the automated creation of 3D models for subsequent finite element analysis. The predictive model generated results consistent with previous studies involving mechanical testing on actual human bones. Notably, the implementation of our predictive model substantially decreased processing time for Finite Element Analysis, rendering it more suitable for clinical use and easier to extend for future application.

Keywords Heterogeneous, CT, Finite element, Fracture, Biomechanics

In the era of global aging, osteoporosis and fragility fractures are becoming significant health concerns[1]. Fragility fractures are associated with increased mortality, morbidity, a decline in quality of life, and substantial economic burden[2,3]. Patients with osteoporosis have a more fragile bone tissue structure due to weakened bones, leading to an increased risk of fragility fractures in the spine due to changes in bone quality.

Clinically, osteoporosis is often diagnosed by measuring Bone Mineral Density (BMD) using Dual-energy X-ray Absorptiometry (DXA). However, this method has two limitations: The first is that the additional cost of DXA results in lower diagnostic testing rate, with only 9.5% of eligible Medicare women and 1.7% of men receiving DXA diagnostic screening for osteoporosis in the United States each year[4]. The second limitation is that BMD measurements by DXA cannot directly estimate the bone strength of osteoporosis patients. Although bone strength is indeed related to BMD[5], DXA-derived BMD measurements do not account for important

[1]Department of Biomedical Engineering, College of Engineering, Chang Gung University, Taoyuan 33302, Taiwan. [2]Bone and Joint Research Center, Department of Orthopedic Surgery, Linkou Chang-Gung Memorial Hospital, Taoyuan 33305, Taiwan. [3]Department of Biomedical Engineering, National Yang Ming Chiao Tung University, Taipei 112, Taiwan. [4]Hsiang-Ho Chen and Chieh-Wei Wu contributed equally to this work. ✉email: polianglai@gmail.com

biomechanical factors of bone strength, such as the shape and three-dimensional geometry of the bone, the relation between cortical and trabecular bone, variations in local cortical thickness, and the internal spatial distribution of bone density. Therefore, DXA has limitations in accurately predicting fracture risk[6,7].

Finite Element Analysis (FEA) is widely used in biomechanical research. It involves discretizing an object into finite sub-elements through meshing and calculating the stiffness matrix of each node during mechanical loading, based on given material properties, boundary conditions, and contact behavior. In medicine, FEA is commonly applied in areas such as implant development, hemodynamics, sports injury assessment, and procedural simulation[8–11]. The principal strain at the yield strength is considered an important indicator of this risk. Based on the results of FEA, it can assist in predicting and evaluating the patient's fracture risk[12].

A clinically validated and convenient diagnostic test for osteoporosis, now available for clinical use in the United States, employs non-invasive assessment of bone strength, serving as a medical insurance benefit for osteoporosis[13]. The American Medical Association officially refers to this as "Biomechanical Computed Tomography (BCT) analysis," which includes bone strength Finite Element Analysis using clinical resolution CT scans as input[14]. It also involves measuring CT-based BMD and DXA-equivalent hip BMD T-scores. Originally developed in 1991[15], BCT has been further validated through various studies and reviews[16,17], the Finite Element Analysis component of BCT represents a "virtual stress test," enabling functional, non-invasive assessment of fracture strength in patients[18,19]. BCT utilizes data from a patient's CT scans as input, performing a virtual stress test to calculate measurements of bone strength. Bone strength is quantified as the force (in Newtons) required to fracture or break the patient's hip or spine under a standard load.

A major drawback of FEA is its high computational and time cost. The quality, quantity, and size of the mesh affect the time cost of the operation. Increasing the number of meshes leads to more accurate results, with the outcomes tending towards a stable convergent value. However, the time taken for computation increases with the number of meshes. The design of the mesh significantly impacts both the accuracy and reliability of FEA results. Therefore, if FEA is to be applied in clinical diagnosis, overcoming the manual labor costs involved in FEA preprocessing is essential.

In recent years, Finite element modelling from CT has been developed over the past few decades. Dao et al.'s study employed a semi-automatic segmentation method based on threshold principles to create three-dimensional geometries of the lumbar spine skeleton by utilizing the ScanIP module (Simpleware, UK)[20]. This approach effectively distinguished the spine from surrounding tissues. Subsequently, they generated 3D Stereolithography (STL)-based geometries, which were then prepared for further processing. Demir et al's study utilized an open-source software to process CT images and facilitate the export of models in STL format[21]. With this, a CAD program can be employed to refine the surface smoothness and to construct intervertebral components.

In FEA modeling, there's a common practice of assuming materials to be uniformly homogeneous[22–24], which often results in the exaggerated calculation of stress levels[25]. Alternatively, CT scans can be used to assign distinct mechanical properties to different regions of the bone, reflecting variations in density and elasticity. This approach facilitates the development of bone-specific FE models to construct individualized bone models and enables the simulation of bone stress under diverse loading scenarios[26,27]. However, the current methodologies in the creation of spine skeleton models by CT images reveal a limitation in the dependence on manual intervention for achieving model perfection. This dependency not only complicates the process but also introduces potential human error and variability in the final model.

The purpose of this study is to construct a predictive FE model for vertebral bodies based on individualized CT images, establishing the structural strength of vertebral bodies, and predicting the risk of vertebral fractures. This patient-specific finite element model was as heterogeneous as real bony structure and generated automatically to reduce the time and computational costs, while also minimizing variability introduced by human intervention. To validate our FE model's predictions and assess its clinical applicability, a comparison of biomechanical differences between the two gender groups in subjects over 50 years of age was performed through our FEA procedure. A 10-year prospective population-based study has demonstrated a significant difference in Bone Mineral Density (BMD) across genders in individuals over the age of 50[28]. Uniaxial compressive properties of human L1 vertebrae were compared between the two gender groups in subjects over 50 years of age by Yeni et al. in 2022[29]. Could our predictive model offer a useful alternative for assessing spinal strength and its fracture risk in patients undergoing CT examination, given similar findings from these studies?

Materials and methods
Patient cohort
This study was a retrospective data analysis. The requirement for informed consent was waived by the institutional review board (IRB) due to the nature of the study, as it involved only the analysis of previously collected and anonymized data. The research protocol was reviewed and approved by Chang Gung Medical Foundation Institutional Review Board, IRB No.: 202200744B0. The study utilized medical records and associated medical images from the Chang Gung Memorial Research Database (CGRD), which collected data from patients with informed consent obtained at the time of data collection. Inclusion criteria were persons aged 50 years and above. The exclusion criteria were persons experience L1 fracture within 3 months and has experience implantation. All methods were performed in accordance with the relevant guidelines and regulations.

CT examinations
CT examinations were performed at Chang Gung Memorial Hospital. Briefly, chest and or abdominal CT examinations were performed by using a variety of multi-detector CT scanners from TOSHIBA (Tokyo, Japan). It had a peak voltage of 120 kV and had variable tube current values from 530 mA to 88 mA that were

protocol-specific but clinically suitable to achieve the diagnostic examination for a given indication.The imaging parameters included a pixel spacing of 0.4 x 0.4 mm^2 and a slice thickness of 3 mm.

Model construction

CT imaging data were processed through a series of steps in MATLAB R2023b (The MathWorks, Inc., Natick, Massachusetts, USA) to prepare them for analysis. Initially, the data were transformed into Hounsfield Units (HU) for standardization, smoothed and flipped to enhance image quality. A three-dimensional matrix was constructed by stacking a series of CT images. Then, DICOM information was extracted and smoothed to reduce image noise, and improved clarity by using MATLAB's functions. Image segmentation was performed, involving the adjustment of image thresholds to delineate the vertebral body boundaries. According to Jang et al.'s study, a predefined HU threshold (160) effectively separated vertebral body from cartilage and soft tissue in CT images[30]. The L1 vertebral body was isolated and reconstructed to preserve the integrity of the bone structure in the analysis, ensuring the precision and reliability of the study's findings[31].

Reorientation of images
Creation of an Interactive User Interface: An interactive window was displayed, allowing users to manually select two points on the image, defining the XY plane coordinate for the FE model (Fig. 1a). The normal vector derived from these points establishes a fixed orientation, ensuring alignment along the Z-axis. This axis serves as the principal direction for the applied FEA force, maintaining perpendicularity to the plane of interest. Therefore, the selected vector must be parallel to the surface of the vertebra to ensure proper alignment with the applied force.

Cropping to retain the vertebral body section
In this stage of the study, the user was prompted to select four points, and their coordinates were recorded (Fig. 1b). The convex hull algorithm was applied to create a quadrilateral formed by these four selected points. This convex quadrilateral enclosed the L1 vertebral body, ensuring its precise isolation for further analysis. This user-guided approach allows targeted cropping, enhancing the specificity and accuracy of the extracted regions. The coordinates of the selected points were converted into pixel positions, and MATLAB's built-in 'poly2mask' function was employed for binarizing the image. This process involved assigning a value of 1 to the interior of the convex hull quadrilateral and 0 to the exterior.

Image crack repair and noise reduction
Morphological filtering techniques were applied to repair image cracks and reduce noise[32].The internal holes within the images were effectively filled (Fig. 2). These morphological operations are crucial for enhancing image quality by removing artifacts and inconsistencies, thereby ensuring a more accurate representation of the anatomical structures for subsequent analysis.

(a)

(b)
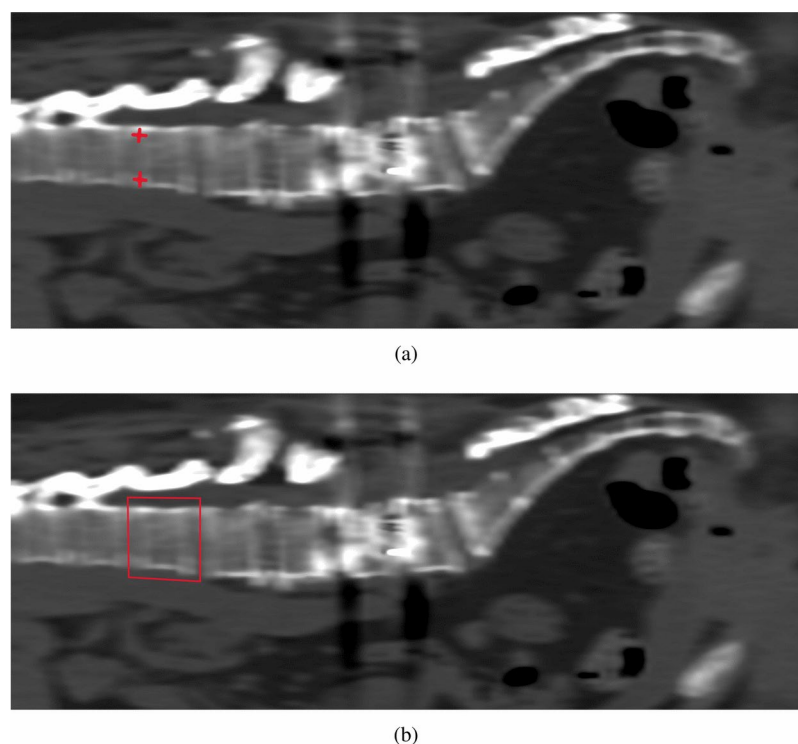
Fig. 1. User interface in MATLAB (**a**) selecting two points to create an axis for image rotation; (**b**) selecting four points to isolate L1 vertebral body.
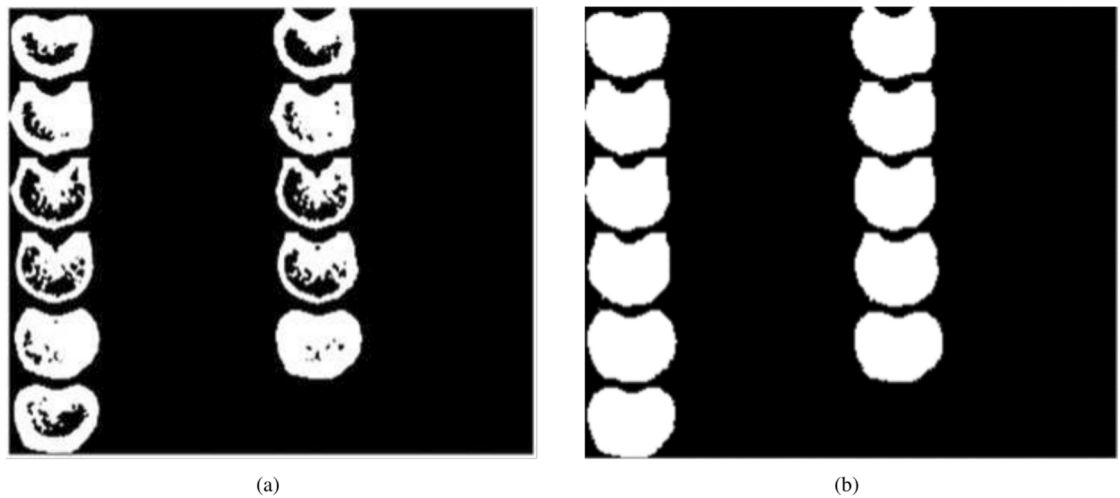
Fig. 2. Image crack repair and noise reduction. (**a**) Internal holes in the vertebral body model; (**b**) the outcome after morphological filtering.
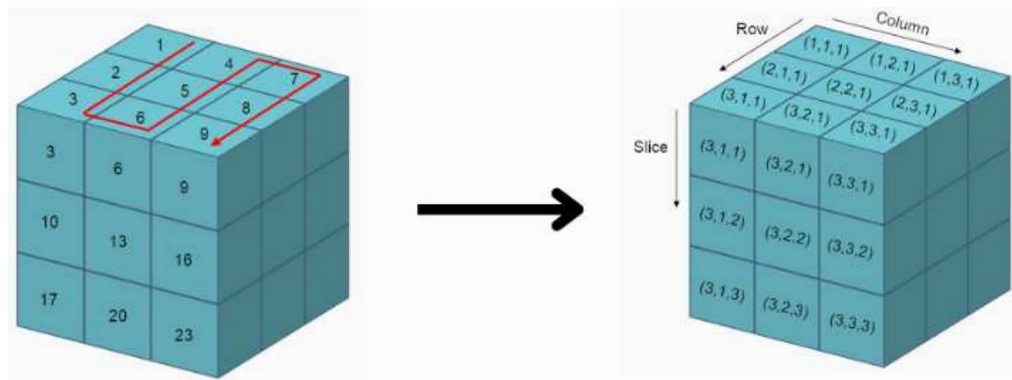
Fig. 3. The typical example about linear indices in three-dimensional space.

Model intensity reconstruction
Linear indices of the voxels were retrieved based on different pixel values corresponding to image intensity (Fig. 3). These indices were then converted into row and column subscripts. Additionally, the location and intensity information of each voxel was systematically recorded and stored.

The next step was to use the acquired image spacing and pixel size to calculate the three-dimensional coordinates of the eight vertices of each voxel. Referring to the following formula provided by Rho et al.'s study[33], the density and elastic modulus of each material were calculated based on its Hounsfield Units.

$$\rho = 1.122 \times \mathrm{HU} + 47$$

$$\mathrm{Elastic\ modulus\ } (E \text{ in MPa}) = 4730 \times \rho^{1.56}$$

This modulus-density relationship has been utilized in various studies for the development of finite element (FE) models of the lumbar spine[34,35]. The various elastic moduli (E) were assigned in models with a linear elastic isotropic behavior for the material properties (Fig. 4).

Voxel-based finite element modeling
All node coordinates, elements containing these nodes, and computed material properties were compiled and exported in the format of a Key file, adhering to the input file specifications of the solver. The FEA solver LS-DYNA R11 (LSTC, Livermore, CA, USA) was employed to determine the distribution of the principal strain and stress in a vertebral body under a distributed load. MATLAB was used to generate LS-DYNA input files.

Boundary conditions applied to the FE model
The boundary conditions were imposed to the vertebral body (Fig. 5). A uniformly distributed force of 1000N was vertically loaded on the upper endplate surface of the vertebral body. Additionally, the six degrees of freedom on the lower surface of the spine were constrained.
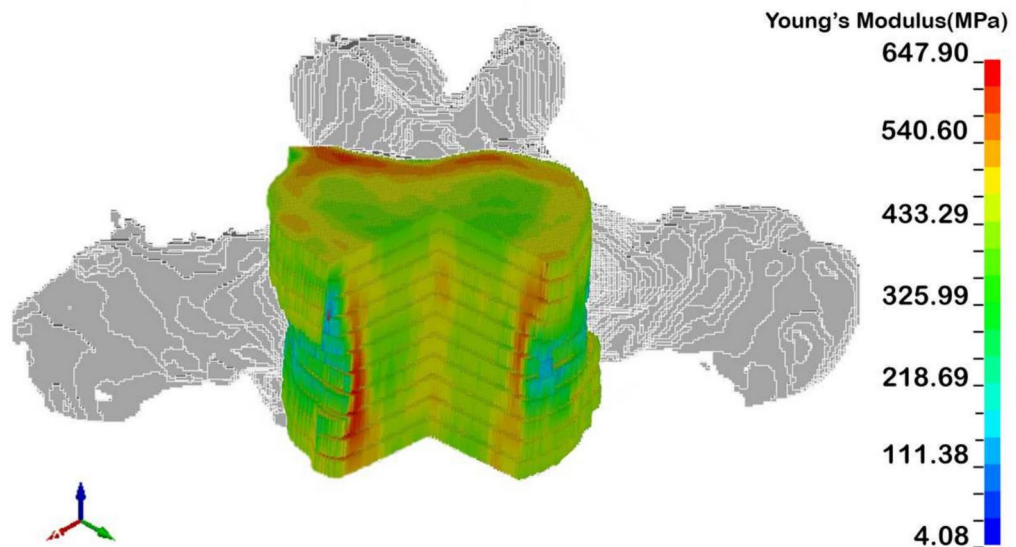
Fig. 4. The distribution of elastic moduli in the vertebral body model.

Fig. 5. The distribution of the force applied on the vertebral body. (**a**) The grey arrows on the red area represent the 1000 N force exerted on the upper surface; (**b**) the blue area represents the fully constrained lower surface with 6 degrees of freedom.

Statistical analysis

In this study, statistical analyses were performed using IBM SPSS Statistics Version 26. The parametric method of the unpaired Student's t-test was employed because the data followed a normal distribution. For all tests, the p-value of 0.05 was set for the statistical significance. Data are expressed as mean ± standard deviation (SD).

Results

A total of 52 spinal CT imaging datasets were systematically collected from volunteer patients at Chang Gung Memorial Hospital, Taiwan. This included 28 male and 24 female participants, with ages ranging from 50 to 95 years. The average age was 67.0 ± 10.25 years in males and 66.0 ± 11.11 years in females (Table 1). BMI was 25.5 ± 3.66 for males and 26.6 ± 4.50 in females. The incidence of fractures after the age of 50 was 20 cases (71%) in males and 12 cases (50%) in females. Among all participants, 11 (39%) males and 13 (54%) females underwent the BMD test. Osteopenia was diagnosed in one male and one female, whereas osteoporosis was diagnosed in four males and nine females. When loading a 1000N compression force, the results revealed the distribution of von Mises stress (Effective stress), the 1st Principal Strain (tensile), the 3rd Principal Strain (compressive) (Fig. 6). Models with different sizes of meshing were compared to understand the suitability of element meshing. Effective stress data converged when the element size was eight times larger than a single voxel (Fig. 7). To prevent from unique high values due to the surface roughness, the average value of the top 1% of data in the entire vertebral body was selected to represent its maximum value. Additionally, the time required for both the modeling process and finite element analysis was recorded.

The average time required to perform mechanical analyses on a single subject, including MATLAB model construction and the LS-DYNA solver, was 579.6 (± 480.8) s, with a range of 118.2–2035 s. Additionally, data

	Male (n = 28) n (%)	Female (n = 24) n (%)
Demographics		
Age	67.0 (± 10.25)	66.0 (± 11.11)
BMI	25.5 (± 3.66)	26.6 (± 4.50)
Fractures after age 50	20 (71)	12 (50)
BMD test	11 (39)	13 (54)
BMD outcome		
Diagnosis		
Normal BMD	5	3
Osteopenia	2	3
Osteoporosis	4	1
Lumbar spine		
BMD (g/cm^2)	0.932 (0.75 to 1.139)	0.774 (0.55 to 1.02)
T-score	− 0.5 (− 2.2 to 1.9)	− 2.05 (− 4.3 to 0.2)
Z-score	0.427 (− 0.9 to 2.6)	0.138 (− 1 to 1.3)

Table 1. Characteristics, demographic and BMD in 32 subjects over 50 years. BMI, body mass index; BMD, bone mineral density.

transfer from the CT scan required an extra 180 s. A biomechanical comparison was conducted between the male and female groups (Table 2). In the 50–59 age group, the study involved seven males with an average effective stress of 55,013 Pa, the 1st principal strain of 0.044%, the 3rd principal strain of − 0.129%. In comparison, eight females in the same age group exhibited higher stress and strain values, with an average effective stress of 72,991 Pa, the 1st principal strain of 0.084%, the 3rd principal of − 0.232%. This pattern of higher stress and strain values in females compared to males continues across the older age groups. In the 60–69 age group, 11 males showed an average effective stress of 59,532 Pa and strain values of 0.054% (1st strain) and − 0.159% (3rd strain). Conversely, nine females in this age group demonstrated significantly higher stress (95,924 Pa) and strain values (0.100% and − 0.277%). The overall average across all age groups indicated that males had an average effective stress of 58,392 Pa with a standard deviation of ± 12,263, and principal strain of 0.055% (± 0.022) and − 0.153% (± 0.053). In contrast, females displayed a significantly higher average effective stress of 83,044 Pa (± 20,422) and principal strain of 0.094% (± 0.023) and − 0.267% (± 0.050).

Discussion

Patient-specific finite element analysis can provide a more detailed assessment of bone strength to complement traditional clinical methods, such as bone mineral density (BMD) assessments using dual-energy X-ray absorptiometry (DXA). However, its application is limited by modeling complexity and high computational requirements. This study focused on simplifying preprocessing steps to reduce time and computational costs while minimizing subjective effects caused by manual work. The L1 vertebrae of 28 male and 24 female participants aged 50–95 years were analyzed using our FEA procedure. The modulus-density relationship used in this study was further analyzed through a sensitivity analysis involving eight subjects, assessing the influence of parameter variations in the formula. When the exponent was adjusted from 1.56 to 1.46 (difference: − 0.1), the effective stress exhibited a rate of change of 5.23% ± 4.92%, indicating a moderate sensitivity of this parameter. In contrast, a slight modification of the multiplier from 4730 to 4729 (difference: − 1) resulted in a negligible change in the effective stress calculation, with a rate of change of less than 0.01%. This can provide a reference for utilizing a suitable formula for the modulus-density relationship on mechanical simulation.

In this study, the cortical shell of the vertebrae was identified from sagittal plane CT scans using a binarization process, which effectively distinguished bony structures from surrounding soft tissues. This segmentation method ensures selection of cortical bone regions. According to Panjabi et al., the cortical shell thickness of human cervical vertebral bodies ranges from 0.44 to 0.89 mm[36]. Given that the voxel resolution in this study was $0.4 \times 0.4 \times 3$ mm^3, the cortical shell could be identified and modeled within the resolution of the imaging and segmentation protocols.

The biomechanical analysis predicted that the average effective stress and principal strain in the female group were significantly higher than in the male group. This finding suggests that women over 50 years of age have a higher fracture risk than men. In this biomechanical analysis, von Mises stress, 1st principal strain, and 3rd principal strain of the vertebrae were compared between genders. The analysis revealed a significant difference between males and females in this age group (Fig. 8). The increase in strain and stress under a 1000 N compressive load suggests that the bone tissue of these individuals experienced greater internal deformation, increasing the risk of structural failure[37]. Women over 50 years of age tend to exhibit higher von Mises stress and increased strain levels. This phenomenon can be attributed to age-related bone density loss, commonly observed in postmenopausal women due to hormonal changes, particularly the decline in estrogen levels[38].

To predict the occurrence of femoral neck fractures, a maximum principal strain criterion has been validated in vitro and successfully applied in vivo[39–41]. Based on this, FE-strength was defined as the load causing a principal strain greater than the limit value (0.73 % tensile limit strain, 1.04 % compressive) in the femoral neck surface[39,42]. To investigate human vertebral strength, Yeni et al. conducted uniaxial compression testing on 27

(a)

(b)

(c)
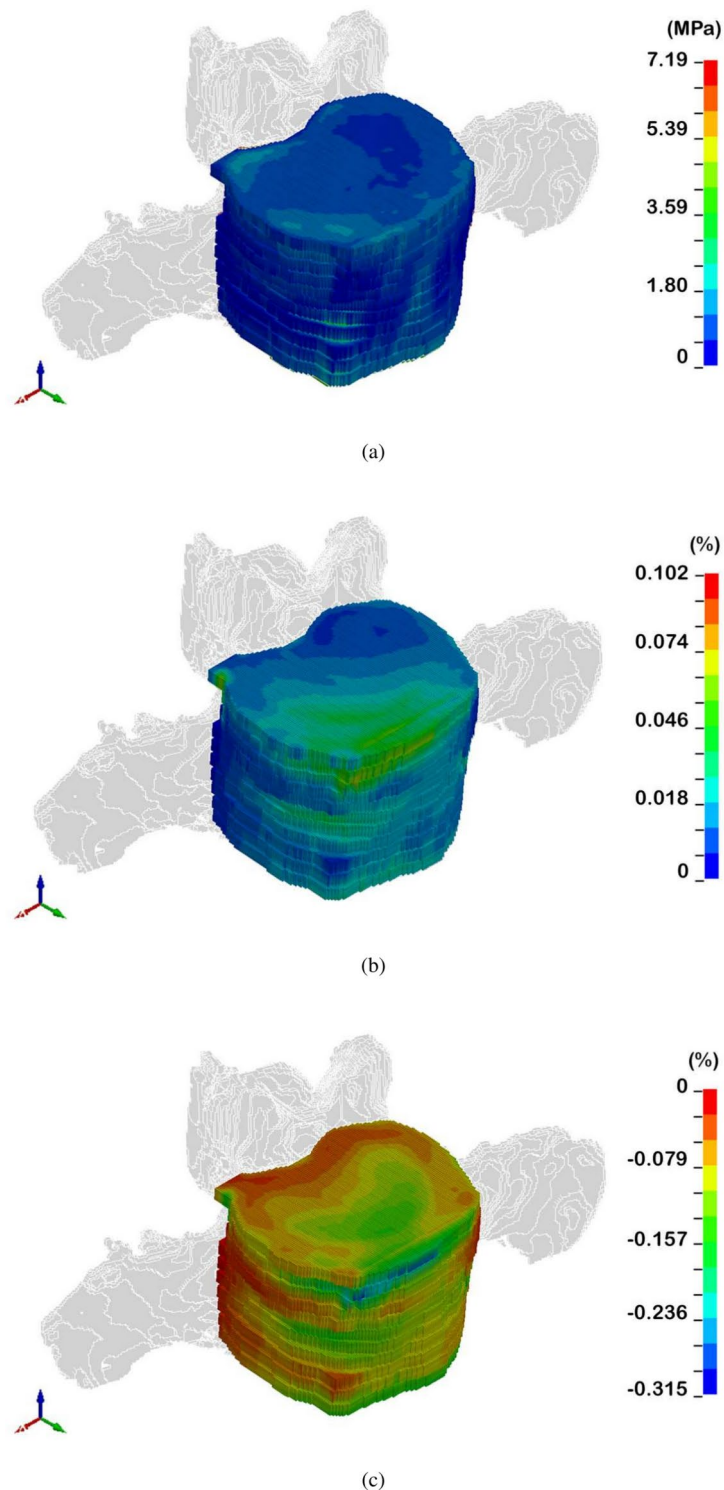
Fig. 6. The typical results include distribution contours of: (**a**) von Mises stress (MPa), (**b**) 1st Principal Strain (%), (**c**) 3rd Principal Strain (%) under the loading force 1000N at L1 vertebral body.

cadaveric L1 vertebrae and found that the average failure force was 4657 ± 1230 N in males and 3197 ± 1260 N in females[29]. Another study by Schröder et al. examined 13 body donors with osteoporosis and reported an average failure force at L1 of 3051 ± 1205 N in males and 2358 ± 1150 N in females[43]. In this study, the average FE-strength of L1 vertebrae was 7755 ± 2926 N in males and 4056 ± 879 N in females. Based on similar findings regarding gender differences in the literature and clinical observations, our predictive model may provide a useful alternative for assessing the risk of spinal failure in patients undergoing CT examinations.
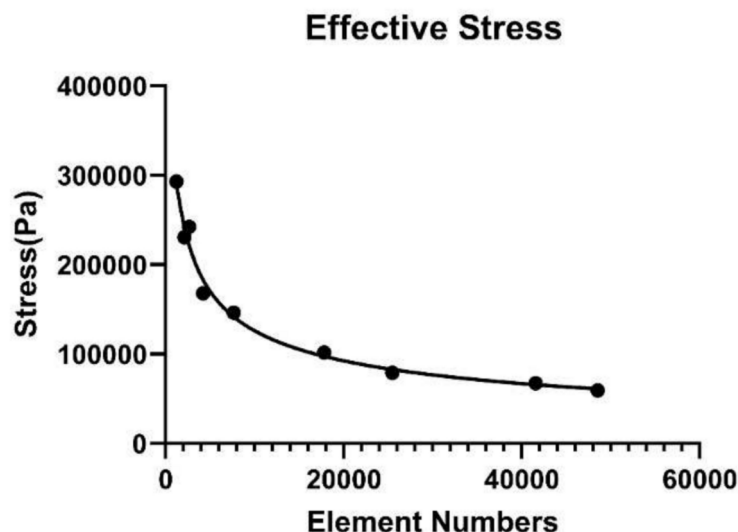
Effective Stress

Fig. 7. The convergence test: a comparison of peak effective stress of models with different element numbers.

	Male (in average)				Female (in average)			
	n	Effective stress (Pa)	1st strain (%)	3rd strain (%)	n	Effective stress (Pa)	1st strain (%)	3rd strain (%)
50–59 age	7	55,013	0.044	− 0.129	8	72,991	0.084	− 0.232
60–69 age	11	59,532	0.054	− 0.159	9	95,924	0.100	− 0.277
70–79 age	7	63,345	0.071	− 0.179	3	74,450	0.087	− 0.254
> 79 age	3	50,540	0.045	− 0.121	4	80,613	0.106	− 0.324
All	28	58,392 (± 12,263)	0.055 (± 0.022)	− 0.153 (± 0.053)	24	83,044 (± 20,422)	0.094 (± 0.023)	− 0.267 (± 0.050)

Table 2. Biomechanical comparison of L1 vertebral body in different age and gender groups by FEA. Compressive loading: 1000 N.

(a)

(b)

(c)
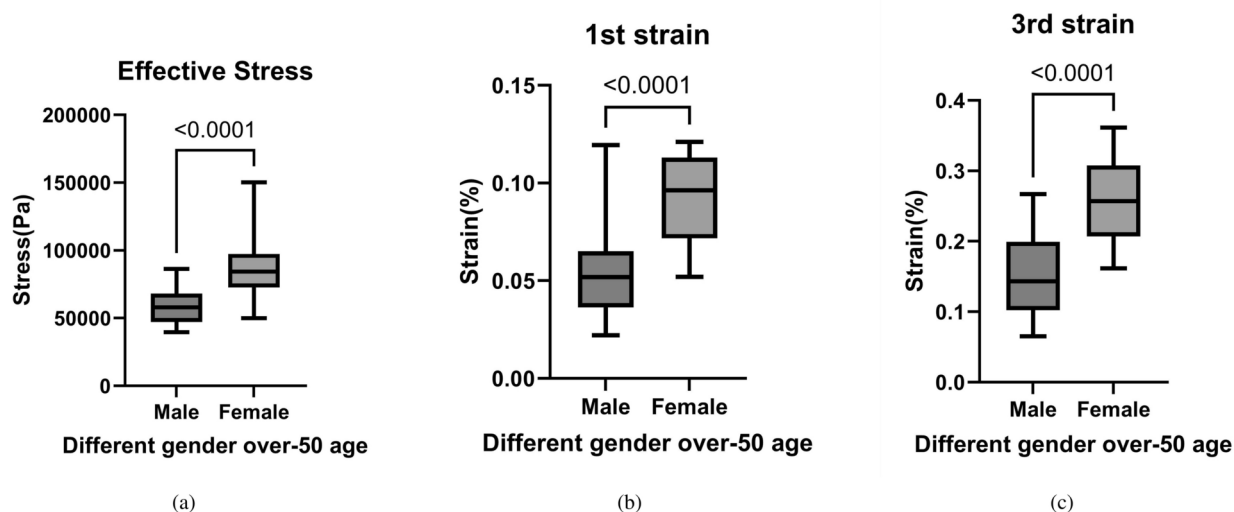
Fig. 8. Comparative analysis of biomechanical parameters between males and females: (**a**) von Mises stress, (**b**) 1st principal strain, (**c**) 3rd principal strain. Significant differences indicated by P Value < 0.05.

Voxel-based models were employed in our prediction procedure to achieve the most realistic distribution of heterogeneous bone possible. Regarding the predictions of our FE model, the displacement of the L1 vertebral body was 0.245 ± 0.096 mm in males and 0.258 ± 0.081 mm in females under the failure force. In contrast to the findings of Yeni et al. (2022), who reported displacements of 0.734 mm and 0.703 mm for males and females, respectively, under compressive loads of 4657 N and 3197 N in their experiments. This study suggests that the observed changes in displacement may be linked to variations in mean vertebral height and cross-sectional area within our sample (Table 3). These anatomical differences in our results are primarily attributed to variations in the structural dimensions of the analyzed vertebral bodies.

An assessment of inter and intra-user variability was conducted to have a better control of manual processing. Each intra-user assessment was performed four times by the same individual to ensure consistency, while the inter-user variability was assessed between two different users assigned. The results of equivalent stress estimation indicate that the intra-user variability exhibited a 0.64% ± 0.48% deviation relative to the mean across the four trials, whereas the inter-user variability demonstrated a 0.94% ± 0.36% deviation between the two users.

This prediction procedure used voxel-based models to simulate heterogeneous characteristics of cancellous bone in the vertebral body. It caused calculation more time-consuming due to larger number of nodes and elements. The recent study published by Nispel et al. (2025) reported that a single vertebra FEM simulation required approximately 2046.73 seconds to complete, using a computer equipped with an Intel i7 CPU with 8 cores, 64 GB of RAM, and a Windows operating system[44]. Additionally, another study by Giambini et al. (2016) developed a finite element model (FEM) using cadaveric L3 vertebrae (three specimens) obtained from CT scans, with a computational time of approximately 8 h on a workstation equipped with an Intel Xeon L5520 (8 CPUs) and 24 GB RAM[45]. In this study, a computer equipped with an Intel Core i5 CPU (4 cores), 16 GB of RAM, and a Windows operating system was used. The average CPU time required to perform mechanical analyses on a single subject, including MATLAB model construction and the LS-DYNA solver, was an average in 579.6 (± 480.8) s (Fig. 9). The numbers of CT images ranged from 26 to 254. The computer calculation time is significantly reduced. The reasons for shortening the time were that high-density elements were used to describe the real inhomogeneous bone distribution, and the direct focus on the trabecular bone compression simulation of the L1 vertebral body simplified the calculation procedure and improved the prediction efficiency. However, extra time about 180 s. for transferring data from CT scan was needed now and hope to be saved in the future.

The average of the top 1% of values could represent a reasonable estimate of FE-strength within the range of experimentally measured failure loads[29,46]. In addition to vertebrae, this CT-based finite element modeling is applicable to improve fracture risk prediction at various skeletal sites, including the proximal femur and distal radius. The proximal femur was analyzed in literature because femoral fractures were common and severe in the elderly. Fully automated segmentation of the proximal femur has received less attention because its less complex shape is easier to extract from CT scans[47]. However, high-quality CT scans are necessary for accurate FEM analysis, which may not be readily available in all clinical settings. Extending these methods with machine learning algorithms for the automatic identification of pathological tissues and biases due to contrast agents could further improve the robustness of this loading-related assessment of fracture risk[48].

The prediction ability of the models can be used to compare with other well-known predictors[49]. However, predictive ability studies need prospective cohort studies with many years of follow-up to monitor for the occurrence of vertebral fractures[50]. Also, baseline data based on a larger sample size of participants were important for this regression analysis. That's why few studies have tested the ability of FEA-estimated bone strength to predict vertebral fracture risk[51]. This study did not include long-term follow-up to monitor the occurrence of vertebral fractures in participants. Consequently, the existing fracture events that occurred prior to the CT scans could not accurately represent the risk of future fractures. As a result, this study did not demonstrate the predictive ability of the models developed. For future research, a prospective cohort study can be conducted to evaluate the relationship between this model and the risk of new vertebral fractures. However, the manual intervention in transition process from MATLAB to LS-DYNA for the FE analyses has not been saved yet due to different system and scaling of imaging. This limitation highlights the need for further development of streamlined analytical workflows and deep learning to improve the efficiency and applicability of this approach.

Additionally, The elastic modulus of bone was determined by the modulus-density formula used in this study. The formula for the Young's modulus-density relationship used demonstrates a higher accuracy ($R^2 > 0.6$) for the cancellous bone, but have lower correlation for cortical bone predictions ($R^2 < 0.2$)[33]. Based on fracture mechanics, fracture is more likely decided by a weaker and main part in a whole structure, such as the cancellous bone in the vertebral body. Therefore, this limitation for simulating the cortical bone may not affect the fracture predictions presented in this study.

	Our result		Yeni et al. in 2022	
	Male (N = 28)	Female (N = 24)	Male (N = 15)	Female (N = 12)
Age (Years)	67.0 ± 10.25	66.0 ± 11.11	63.9 ± 11.1	71.5 ± 18.3
Failure force (N)	7755 ± 2926	4056 ± 879	4657 ± 1230	3197 ± 1260
Displacement to failure (mm)	0.245 ± 0.096	0.258 ± 0.081	0.734 ± 0.197	0.703 ± 0.209
Vertebral height (mm)	34.9 ± 5.8	34.8 ± 7.6	47.0 ± 3.1	43.0 ± 4.6
HRCT AP Width (mm)	50.7 ± 5.1	46.4 ± 9.1	52.5 ± 4.8	50.6 ± 8.5
HRCT LM Width (mm)	36.5 ± 3.6	33.6 ± 4.1	44.2 ± 4.7	42.3 ± 4.8

Table 3. Comparison of biomechanical characteristics between our result and Yeni et al. in 2022.
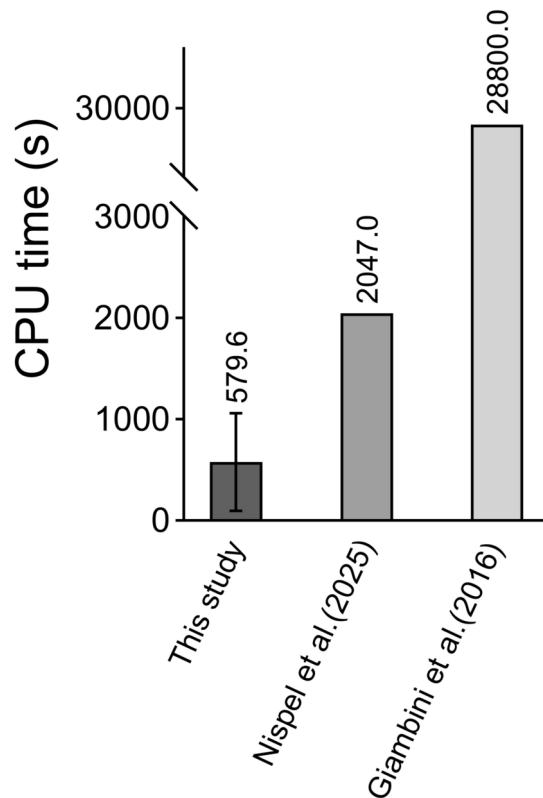
Fig. 9. Comparison of computational time across different studies on vertebral finite element modeling.

The present study used subjects from an Asian population; however, there is limited literature proposing equations for vertebral density-elasticity relationships specific to Asian populations. Kepley et al. (2017) studied femoral samples from young individuals and reported that Asians have smaller bones, thicker and denser cortices, and more plate-like trabeculae, but stiffness did not differ between groups[52]. A newer density-elasticity relationship formula for Asian vertebrae may improve the accuracy of this fracture risk prediction in the future.

Conclusions

This study demonstrates that this procedure has been successfully applied to select specific spinal segments from CT images and automatically generate 3D models for subsequent finite element analysis. Through modeling optimization, the average CPU time required for mechanical analysis was significantly reduced. Therefore, when voxel-based models with minimized elements were adopted in this method, the heterogeneous bone distribution could be simulated as realistically as possible. In a subsequent application, 52 participants over 50 years of age were recruited to test the modeling and analysis process. Our results revealed that under the same external load, the L1 vertebrae of women over 50 years of age experienced higher stress and strain levels, indicating lower bone strength compared to men of the same age. This finding is consistent with previous studies that utilized experimental measurements on cadaveric bone. Furthermore, our predictive model significantly reduced the computation time for finite element analysis, enhancing its suitability for clinical applications and facilitating its broader implementation.

Data availability

The datasets used and/or analyzed during the current study available from the corresponding author on reasonable request. The data that support the findings of this study are available from Chang Gung Memorial Research Database but restrictions apply to the availability of these data, which were used under license for the current study, and so are not publicly available. Data are however available from the corresponding author upon reasonable request and with permission of Chang Gung Memorial Research Database.

References

1. Abrahamsen, B., van Staa, T., Ariely, R., Olson, M. & Cooper, C. Excess mortality following hip fracture: a systematic epidemiological review. *Osteoporos. Int.* **20**, 1633–50. https://doi.org/10.1007/s00198-009-0920-3 (2009).
2. Alvarez-Nebreda, M. L., Jiménez, A. B., Rodríguez, P. & Serra, J. A. Epidemiology of hip fracture in the elderly in Spain. *Bone* **42**, 278–85. https://doi.org/10.1016/j.bone.2007.10.001 (2008).

3. Brauer, C. A., Coca-Perraillon, M., Cutler, D. M. & Rosen, A. B. Incidence and mortality of hip fractures in the united states. *JAMA* **302**, 1573–9. https://doi.org/10.1001/jama.2009.1462 (2009).

4. Zhang, J. et al. Central dxa utilization shifts from office-based to hospital-based settings among medicare beneficiaries in the wake of reimbursement changes. *J. Bone Miner. Res.* **27**, 858–64. https://doi.org/10.1002/jbmr.1534 (2012).

5. Johannesdottir, F. et al. Comparison of non-invasive assessments of strength of the proximal femur. *Bone* **105**, 93–102. https://doi.org/10.1016/j.bone.2017.07.023 (2017).

6. Adams, A. L. et al. Osteoporosis and hip fracture risk from routine computed tomography scans: the fracture, osteoporosis, and ct utilization study (focus). *J. Bone Miner. Res.* **33**, 1291–1301. https://doi.org/10.1002/jbmr.3423 (2018).

7. Jiang, X. et al. Diagnostic accuracy of frax in predicting the 10-year risk of osteoporotic fractures using the usa treatment thresholds: a systematic review and meta-analysis. *Bone* **99**, 20–25. https://doi.org/10.1016/j.bone.2017.02.008 (2017).

8. Ren, X., Qiao, A., Song, H., Song, G. & Jiao, L. Influence of bifurcation angle on in-stent restenosis at the vertebral artery origin: a simulation study of hemodynamics. *J. Med. Biol. Eng.* **36**, 555–562 (2016).

9. Ren, Y. et al. Biomechanical effect of using cement augmentation to prevent proximal junctional kyphosis in long-segment fusion: a finite element study. *J. Med. Biol. Eng.* **43**, 63–73 (2023).

10. Shih, K.-S & Hsu, C.-C. Three-dimensional musculoskeletal model of the lower extremity: integration of gait analysis data with finite element analysis. *J. Med. Biol. Eng.* **42**, 436–444 (2022).

11. Wang, S. et al. Application of a personalized finite element analysis and 3d-printed navigation template in the treatment of femoral neck fracture with cannulated screw. *J. Med. Biol. Eng.* **41**, 934–941 (2021).

12. Hu, B. W., Lv, X., Chen, S. F. & Shao, Z. W. Application of finite element analysis for investigation of intervertebral disc degeneration: from laboratory to clinic. *Curr. Med. Sci.* **39**, 7–15. https://doi.org/10.1007/s11596-019-1993-7 (2019).

13. Keaveny, T. et al. Biomechanical computed tomography analysis (bct) for clinical assessment of osteoporosis. *Osteoporos. Int.* **31**, 1025–1048 (2020).

14. Keaveny, T. M. Biomechanical computed tomography-noninvasive bone strength analysis using clinical computed tomography scans. *Ann. N. Y. Acad. Sci.* **1192**, 57–65 (2010).

15. Faulkner, K. G., Cann, C. E. & Hasegawa, B. H. Effect of bone distribution on vertebral strength: assessment with patient-specific nonlinear finite element analysis. *Radiology* **179**, 669–674 (1991).

16. Johannesdottir, F., Allaire, B. & Bouxsein, M. L. Fracture prediction by computed tomography and finite element analysis: current and future perspectives. *Curr. Osteoporos. Rep.* **16**, 411–422 (2018).

17. Zysset, P. et al. Clinical use of quantitative computed tomography-based finite element analysis of the hip and spine in the management of osteoporosis in adults: the 2015 iscd official positions-part ii. *J. Clin. Densitom.* **18**, 359–392 (2015).

18. Bouxsein, M. et al. Perspectives on the non-invasive evaluation of femoral strength in the assessment of hip fracture risk. *Osteoporos. Int.* **31**, 393–408 (2020).

19. Viceconti, M., Qasim, M., Bhattacharya, P. & Li, X. Are ct-based finite element model predictions of femoral bone strengthening clinically useful?. *Curr. Osteoporos. Rep.* **16**, 216–223 (2018).

20. Dao, T.-T., Pouletaut, P. & Lazáry, A. Multimodal medical imaging fusion for patient specific musculoskeletal modeling of the lumbar spine system in functional posture. *J. Med. Biol. Eng.* https://doi.org/10.1007/s40846-017-0243-3 (2017).

21. Demir, E., Eltes, P., Castro, A. P., Lacroix, D. & Toktas, I. Finite element modelling of hybrid stabilization systems for the human lumbar spine. *Proc. Inst. Mech. Eng. H* **234**, 1409–1420. https://doi.org/10.1177/0954411920946636 (2020).

22. Boström, A., Amin, A. K., Macpherson, G. J., Pankaj, P. & Scott, C. E. H. Hinge location and apical drill holes in opening wedge high tibial osteotomy: a finite element analysis. *J. Orthop. Res.* **39**, 628–636. https://doi.org/10.1002/jor.24704 (2021).

23. Ji, W. et al. Combined proximal tibial osteotomy for varus osteoarthritis of the knee: biomechanical tests and finite-element analyses. *Knee* **27**, 863–870. https://doi.org/10.1016/j.knee.2020.01.006 (2020).

24. Weng, P. W. et al. The effects of tibia profile, distraction angle, and knee load on wedge instability and hinge fracture: a finite element study. *Med. Eng. Phys.* **42**, 48–54. https://doi.org/10.1016/j.medengphy.2017.01.007 (2017).

25. Saghaei, Z. & Hashemi, A. Homogeneous material models can overestimate stresses in high tibial osteotomy: a finite element analysis. *Proc. Inst. Mech. Eng. H* **237**, 224–232. https://doi.org/10.1177/09544119221144811 (2023).

26. Benca, E., Amini, M. & Pahr, D. H. Effect of ct imaging on the accuracy of the finite element modelling in bone. *Eur. Radiol. Exp.* **4**, 51. https://doi.org/10.1186/s41747-020-00180-3 (2020).

27. Kazembakhshi, S. & Luo, Y. Constructing anisotropic finite element model of bone from computed tomography (ct). *Biomed. Mater. Eng.* **24**, 2619–26. https://doi.org/10.3233/bme-141078 (2014).

28. Daly, R. M. et al. Gender specific age-related changes in bone density, muscle strength and functional performance in the elderly: a-10 year prospective population-based study. *BMC Geriatr.* **13**, 71. https://doi.org/10.1186/1471-2318-13-71 (2013).

29. Yeni, Y. N., Dix, M. R., Xiao, A. & Oravec, D. J. Uniaxial compressive properties of human lumbar 1 vertebrae loaded beyond compaction and their relationship to cortical and cancellous microstructure, size and density properties. *J. Mech. Behav. Biomed. Mater.* **133**, 105334. https://doi.org/10.1016/j.jmbbm.2022.105334 (2022).

30. Jang, S. et al. Opportunistic osteoporosis screening at routine abdominal and thoracic ct: normative l1 trabecular attenuation values in more than 20 000 adults. *Radiology* **291**, 360–367. https://doi.org/10.1148/radiol.2019181648 (2019).

31. Zhang, Y. et al. Joined fragment segmentation for fractured bones using gpu-accelerated shape-preserving erosion and dilation. *Med. Biol. Eng. Comput.* **58**, 155–170. https://doi.org/10.1007/s11517-019-02074-y (2020).

32. Vincent, L. Morphological area openings and closings for grey-scale images. In *Shape in Picture: Mathematical Description of Shape in Grey-Level Images* 197–208 (Springer, 1994).

33. Rho, J. Y., Hobatho, M. C. & Ashman, R. B. Relations of mechanical properties to density and ct numbers in human bone. *Med. Eng. Phys.* **17**, 347–55. https://doi.org/10.1016/1350-4533(95)97314-f (1995).

34. Rayudu, N. M. et al. Patient-specific finite element modeling of the whole lumbar spine using clinical routine multi-detector computed tomography (mdct) data-a pilot study. *Biomedicines* **10**, 1567 (2022).

35. Turbucz, M. et al. Development and validation of two intact lumbar spine finite element models for in silico investigations: Comparison of the bone modelling approaches. *Appl. Sci.* **12**, 10256 (2022).

36. Panjabi, M. M., Chen, N. C., Shin, E. K. & Wang, J.-L. The cortical shell architecture of human cervical vertebral bodies. *Spine* **26**, 2478–2484 (2001).

37. Fiorillo, L. et al. Finite element method and von mises investigation on bone response to dynamic stress with a novel conical dental implant connection. *Biomed. Res. Int.* **2020**, 2976067. https://doi.org/10.1155/2020/2976067 (2020).

38. van den Berg, M. et al. Vertebral fractures in women aged 50 years and older with clinical risk factors for fractures in primary care. *Maturitas* **70**, 74–79. https://doi.org/10.1016/j.maturitas.2011.06.006 (2011).

39. Bayraktar, H. H. et al. Comparison of the elastic and yield properties of human femoral trabecular and cortical bone tissue. *J. Biomech.* **37**, 27–35. https://doi.org/10.1016/s0021-9290(03)00257-4 (2004).

40. Falcinelli, C. et al. Multiple loading conditions analysis can improve the association between finite element bone strength estimates and proximal femur fractures: a preliminary study in elderly women. *Bone* **67**, 71–80 (2014).

41. Schileo, E., Taddei, F., Cristofolini, L. & Viceconti, M. Subject-specific finite element models implementing a maximum principal strain criterion are able to estimate failure risk and fracture location on human femurs tested in vitro. *J. Biomech.* **41**, 356–367 (2008).

42. Qasim, M. et al. Patient-specific finite element estimated femur strength as a predictor of the risk of hip fracture: the effect of methodological determinants. *Osteoporos. Int.* **27**, 2815–2822. https://doi.org/10.1007/s00198-016-3597-4 (2016).

43. Schröder, G. et al. Breaking strength and bone microarchitecture in osteoporosis: a biomechanical approximation based on load tests in 104 human vertebrae from the cervical, thoracic, and lumbar spines of 13 body donors. *J. Orthop. Surg. Res.* **17**, 228. https://doi.org/10.1186/s13018-022-03105-5 (2022).

44. Nispel, K. et al. From mri to fem: an automated pipeline for biomechanical simulations of vertebrae and intervertebral discs. *Front. Bioeng. Biotechnol.* **12**, 1485115 (2025).

45. Giambini, H., Qin, X., Dragomir-Daescu, D., An, K.-N. & Nassr, A. Specimen-specific vertebral fracture modeling: a feasibility study using the extended finite element method. *Med. Biol. Eng. Comput.* **54**, 583–593 (2016).

46. Schröder, G. et al. Breaking strength and bone microarchitecture in osteoporosis: a biomechanical approximation based on load tests in 104 human vertebrae from the cervical, thoracic, and lumbar spines of 13 body donors. *J. Orthop. Surg. Res.* **17**, 228 (2022).

47. Kim, J. J., Nam, J. & Jang, I. G. Fully automated segmentation of a hip joint using the patient-specific optimal thresholding and watershed algorithm. *Comput. Methods Programs Biomed.* **154**, 161–171 (2018).

48. Fleps, I. & Morgan, E. F. A review of ct-based fracture risk assessment with finite element modeling and machine learning. *Curr. Osteoporos. Rep.* **20**, 309–319 (2022).

49. Shevroja, E., Mo Costabella, F., Gonzalez Rodriguez, E., Lamy, O. & Hans, D. The fracture predictive ability of lumbar spine bmd and tbs as calculated based on different combinations of the lumbar spine vertebrae. *Arch. Osteoporos.* **17**, 83 (2022).

50. Wang, X. et al. Prediction of new clinical vertebral fractures in elderly men using finite element analysis of ct scans. *J. Bone Miner. Res.* **27**, 808–816 (2012).

51. Allaire, B. et al. Prediction of incident vertebral fracture using ct-based finite element analysis. *Osteoporos. Int.* **30**, 323–331 (2019).

52. Kepley, A. et al. Differences in bone quality and strength between asian and caucasian young men. *Osteoporos. Int.* **28**, 549–558 (2017).

Acknowledgements

Author contributions

Conceptualization, HH.C. and PL.L.; methodology, Y.C. and MC.S.; software, MC.S and YJ.C.; validation, HH.C., CW.W. and PL.L.; formal analysis, CW.W.; investigation, Y.C., MC.S. and YJ.C.; resources, PL.L.; data curation, HH.C. and PL.L.; writing-original draft preparation, CW.W.; writing-review and editing, HH.C. and CW.W.; visualization, CW.W.; drawings in Figures [4,5,6], HH.C., CW.W., and MC.S.; supervision, HH.C. All authors have read and agreed to the published version of the manuscript. HH.C. and CW.W. contributed equally to this work.

Competing interests

The authors declare no competing interests.

Additional information

Correspondence and requests for materials should be addressed to P.-L.L.

Reprints and permissions information is available at www.nature.com/reprints.

Publisher's note Springer Nature remains neutral with regard to jurisdictional claims in published maps and institutional affiliations.